Heterogeneous Integration of Doped Crystalline Zirconium Oxide for Photonic Applications

Alicia Ruiz-Caridad, Guillaume Marcaud, Elena Duran-Valdeiglesias, Joan Manel Ramirez, Jianhao Zhang, Carlos Alonso-Ramos, Xavier Leroux, Ludovic Largeau, Samuel Serna, Nicolas Dubreuil, et al.

Heterogeneous integration of doped crystalline zirconium oxide for photonic application (Invited paper)

Alicia Ruiz-Caridad[1,*], Guillaume Marcaud[1,2,*], Elena Duran-Valdeiglesias [3], Joan Manel Ramirez[4], Jianhao Zhang[1], Carlos Alonso-Ramos[1], Xavier LeRoux[1], Ludovic Largeau[1], Samuel Serna[5], Nicolas Dubreuil [6], Sylvia Matzen[1], Thomas Maroutian[1], Philippe Lecoeur[1], Delphine Marris-Morini [1], Eric Cassan[1], Laurent Vivien[1]

***Abstract*- Hybrid integration of new materials will play a key role in the next photonics revolution, unlocking the development of advanced devices with outstanding performances and innovative functionalities. Functional oxides, thanks to the richness of their physical properties are promising candidates to build active reconfigurable elements in complex circuits. We review in this article our recent work regarding the hybrid integration of Yttria-Stabilized Zirconia (YSZ), a crystalline oxide with transparency from the visible to the mid-IR range with refractive index of about 2.15. YSZ is mostly studied for its high ionic conductivity, epitaxial growth on Si as buffer layer and its chemical stability but we demonstrated that it also holds a great potential in photonics for the development of low-loss waveguides (<2 dB/cm) and complex passive structures. Kerr refractive index of YSZ is in the same order of magnitude than well-known nonlinear materials such as silicon nitride. We explored the implementation of Er^{3+} ions as an active element providing outstanding luminescence in correspondence with C-band of telecommunications. The optical properties of active layers of Er-doped YSZ grown on waveguides in different platforms and under resonant pumping and its propagation losses, modal gain and signal enhancement will be discussed in this paper.**

***Index Terms*- hybrid photonic platform nanophotonics, yttria-stabilized zirconia, nonlinear effects, optical amplification.**

*Contributed equally

[1]Université Paris-Saclay, CNRS, Centre de Nanosciences et Nanotechnologies (C2N), UMR 9001,10 Boulevard 29 Thomas Gobert, 91120 Palaiseau, France.

[2] Yale University, Department of applied physics, 15 prospect street, 06511 New Haven, CT, USA

[3] Almae Technologies, Route de Nozay, 91460 Marcoussis, France

[4] III-V lab, a joint venture from Nokia Bell Labs, Thales and CEA, 1 Avenue Augustin Fresnel, 91767 Palaiseau Cedex, France

[5]Department of Physics, Bridgewater State University, Bridgewater, MA 02325, United States of America 31

[6]LP2N, LP2N, Institut d'Optique Graduate School, CNRS, Univ. Bordeaux, 33400 Talence, France

I. The potential of oxides integration in silicon photonics

Integrated photonics has emerged as a promising technology to address challenges in high-speed and low-power consumption optical communications. Benefiting from the maturity of the complementary metal-oxide semiconductor (CMOS) technology, silicon-based photonics has emerged as a viable solution for large volume applications and has enabled the integration of optical functionalities on-chip, through passive (ultra-low loss waveguides and grating couplers, resonators, filters...) and active devices (optical modulators, photodetectors, isolators...) [1]. The silicon photonics research field is burgeoning very fast and looking now for more diverse applications, from sensing to metrology and data processing, with a strong impulse toward quantum technology. However, silicon has some limitation to fully address all challenges: The indirect nature of its bandgap, its lack of magnetic ordering and its centrosymmetric crystalline unit cell are examples of silicon properties that prevent the development of advanced on-chip functionalities. More generally, even with the recent improvements of thin films growth techniques and nanofabrication technology, there is not a single-material hosting all required properties. Therefore, to achieve its goals, the silicon photonic community is looking toward the hybrid integration of materials.

Among the candidates, silicon nitride (SiN), chalcogenides, III-V, and Germanium, stand up thanks to their unique properties [2], [3], [4], [5]. These material families are suitable for targeted photonics building-blocks like Ge-based photodetectors and III-V-on-Si lasers but are limited for the development of an universal platform offering additional devices (modulators, isolators, memory...). For this purpose, crystalline oxides are very promising because they hosts a rich physic, including complex electronic structures with charge, magnetic and orbital ordering, as well as strong correlations between these degrees of freedom and the lattice [6]. Consequently, one can find in these oxides a large diversity of phenomena, such as ferroelectricity, ferromagnetism, metal to insulator transitions or high temperature superconductivity. Barium

titanate ($BaTiO_3$) and vanadium dioxide (VO_2) are two examples worth mentioning as they have known a successful integration in photonics. The former is a ferroelectric with a high second-order optical nonlinearity, exploited in high-speed and low-power consumption electro-optic modulators[7]. The latter, VO_2, presents a metal-to-insulator transition (MIT) around 60°C that can be used for tunable or reconfigurable photonic devices[8]. Crystalline oxides possess also the unique capability to be stacked in 3D heterostructures, combining their properties or creating new ones at the interfaces [9]. One typical example is the recent demonstration of a hyperbolic metamaterial made from a heterostructure composed of $La_xSr_{1-x}TiO_3/SrTiO_3$, in which the dielectric permittivity changes sign from one crystallographic direction to another at a tunable wavelength[10].

The hybrid integration of high-quality crystalline oxides in silicon-based platform, including Si and SiN, promises a great potential to unlock a myriad of new devices, going well beyond the only field of silicon photonics. The differences of chemical nature and crystalline lattices between oxides and silicon is, however, an obstacle that we must overcome. Defects in the lattices, alloy formation or interdiffusion at the interface during thin film growth are examples that can lead to the degradation of the material properties. The technological progresses of the past decade have provided solutions for this kind of integration, like the wafer bonding technique, but additional and somehow complex steps are required along the process of fabrication. An interested reader can refer to [11] as an example of this method for the integration of crystalline ferroelectric $BaTiO_3$ for energy storage application. Another approach consists of using of a buffer layer, i.e. a thin layer of material at the interface between the oxide and silicon, to adapt the lattice from silicon to other functional oxides and acting as a barrier for interdiffusion [12]. This buffer material must be compatible with silicon and most of the oxides, very stable to prevent any alloy formation, and grow with high quality to prevent additional limitations to the device. Strontium titanate ($SrTiO_3$) and yttria-stabilized zirconia (Y_2O_3:ZrO_2) are two standard buffer layers well-known in the oxides community to grow oxide thin films on silicon. The former has been extensively studied as the prototypical ABO_3 perovskite, used as a substrate to grow complex oxides or as a buffer layer for $LaAlO_3$ or $BaTiO_3$ on silicon[13]. The latter is known for its thermal and chemical stability, hardness, durability[14] and ionic conductivity. Hence, YSZ has been used as an electrolyte in solid oxide fuel cells (SOFC) and as oxygen sensors[15], [16]. YSZ is also well known as a buffer layer for the growth of functional oxides on silicon[17], [18]. These materials are the keystones towards the hybrid integration of oxides in silicon photonics and therefore must be thoroughly characterized in integrated optics. We present in this review paper the potential of YSZ in integrated optics. The first section introduces the process that we developed to make photonic components out of a YSZ thin film, while the second and third part discuss recent results regarding the non-linear optical properties of YSZ waveguides and the potential of Erbium-doped YSZ (Er:YSZ) in light emitting devices.

II. YSZ THIN FILMS FOR PHOTONICS

Y_2O_3-stabilized ZrO_2 (YSZ) or $(ZrO_2)_{1-x}(Y_2O_3)_x$ is a ceramic with the CaF_2 structure for a wide range of stoichiometric x values. In YSZ, yttrium substitutes a % of zirconium that determines the YSZ crystalline structure, tetragonal or cubic [19]. The cubic phase is preferred due to its lattice constant (a=5.143) similar to that of Si (a=5.431). Besides, YSZ optical properties include: (i) large transparency window from ultraviolet (UV) to mid-IR spectral region, (ii) absence of two photon absorption (TPA) in the near- and mid-infrared wavelengths (near-IR and mid-IR), and (iii) mid-refractive index contrast material (MiDex).

There are typically two complementary approaches to optimize the integration of a new material into a device. The first one focus on the material deposition and patterning processes to understand and reduce the intrinsic limitations of the device induced during its fabrication. The second approach aim to optimize the design of the component to lower the participation of the known limiting mechanisms. We present in this first section how these two methods have been applied to improve the performances of YSZ-based waveguides, when integrated on sapphire and silicon platform.

A. Yttria-Stabilized Zirconia on sapphire

The growth of YSZ is performed using Pulsed-Laser Deposition (PLD), a Physical Vapor Deposition (PVD) technique that employ a powerful pulsed-laser in the UV to transfer a material from a target to a substrate. This method combines the potential of single-crystal-quality growth of thin film, with the possibility to conserve the complex stoichiometry of oxides and the capability to grow thicker film of about several hundreds of nanometers, typical dimensions of waveguides in the near-infrared. More details about the technique can be found in several review paper [20], [21]. To determine the capability of YSZ in integrated optics, we have first considered sapphire substrate (Al_2O_3). This substrate is transparent from visible to mid-IR and has a refractive index of n_{saph}=1.74 at a wavelength of 1.55 μm, lower than YSZ n_{YSZ}=2.15 at the same wavelength [22]. Such a refractive index contrast between the film (YSZ) ans the substrate (sapphire) unlocks the possibility to confine light in YSZ waveguides on sapphire.

The growth parameters studied in this work, as well as the characterization feedback loop are presented in the outer and inner loop of Fig. 1, respectively. We used Atomic-Force Microscopy (AFM) to quantify the roughness of the films, and X-Ray Diffraction (XRD) and transmission Electron Miscroscopy (TEM) to measure the lattice parameter distribution, mosaicity and grains orientation (out-of-plane and in-plane). X-Ray Reflectivity (XRR) and ellipsometry gave us access to the film thicknesses, roughness, density, and optical constants from 400 to 1700 nm. Following

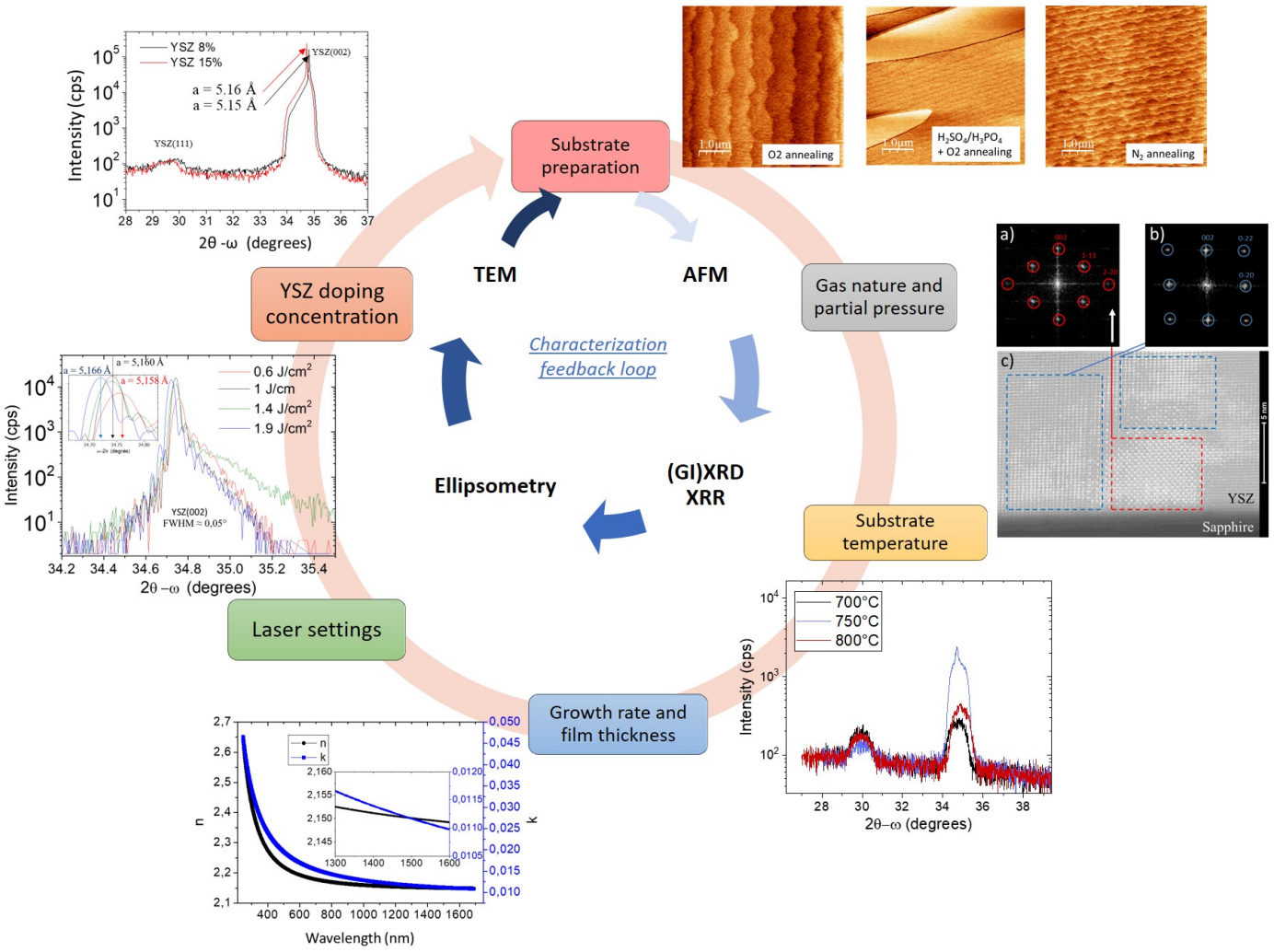

Fig. 1. Parameters optimized in this study (outer loop) and characterization feedback loop (inner loop) for the PLD growth of YSZ on sapphire. The roughness is measured by Atomic-Force Microscopy (AFM). The lattice parameter distribution, mosaicity and crystal orientation (out-of-plane and in-plane) of the films by (Grazing-Incidence) X-Ray Diffraction (GI-XRD) and transmission Electron Miscroscopy (TEM). The fitting of X-Ray Reflectivity (XRR) and ellipsometry data are used to extract film thickness, roughness, density, and optical constant (refactive index and absorption from 400 to 1700 nm). The substrate preparation has the strongest effect on the YSZ growth direction and crystallinity.

this methodology, we are able to determine the effects of the growth condition (vacuum quality, reactive gas nature and pressure, substrate temperature, laser fluence...) to the metrics of the material (phase, defects type and density...), and the relevant combination of these metrics to improve the device's figure of merit.

For the sake of brevity, we will not discuss here all the different data and parameter variation but we can notice that the substrate preparations before growth have the greatest effect on the films' crystallinity and orientation. Indeed, the annealing of the substrate at 1200°C for 4 hours under oxygen or nitrogen before the growth, promote the (001) or (111) growth direction, respectively, and led to the sharpest (10^{-3}°) XRD rocking curve peaks ever reported (i.e. lowest mosaicity)[23]. These types of high-quality and highly oriented films can be grown if the thickness is kept under 350 nm. For thicker films, the rocking curves rapidly broaden and reach 1° at 500 nm, defining an upper thickness limit of 350 nm for the optimal fabrication of devices (see central plot Fig. 3). The other optimized parameters are, a substrate temperature of 800°C, a reactive gas during the growth composed of pure oxygen at a pressure of 30 mTorr, a laser fluence and a repetition rate of 1.9 J/cm^2 and 5 Hz, respectively. Equivalent material quality has been obtained with 8%mol or 15%mol Y_2O_3-doped YSZ.

In parallel to the material optimization, we developed a process of fabrication in cleanroom that considers the specificity of the platform YSZ on sapphire. We developed a process based on electron-beam lithography and Ion-Beam Etching (IBE), and customized to the YSZ and sapphire insulating properties as well as their known hardness and chemical stability. The results of this process is presented Fig. 2 a) with an optical view of a YSZ chip, made of a 300 nm thick YSZ film. All the structures, including waveguides, grating couplers, ring and microdisk resonators, Mach–Zehnder Interferometer (MZI) and sub-wavelength

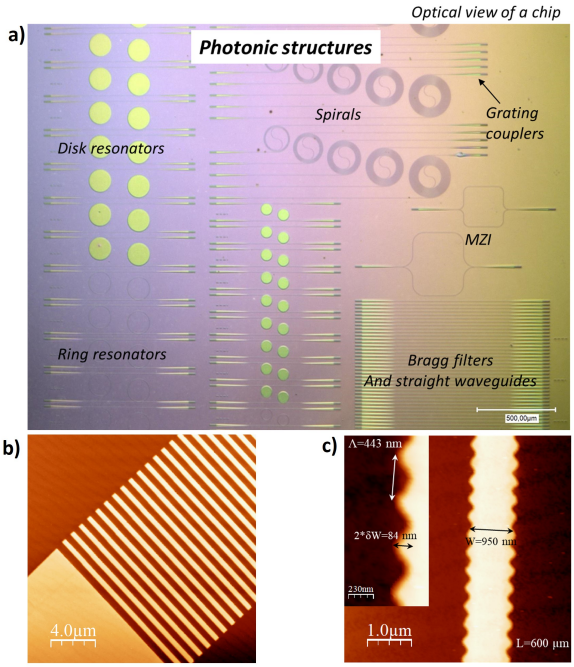

Fig. 2. a) Optical view of a YSZ-based photonic chip on sapphire substrate. The process combines high-resolution e-beam lithography and Ion-Beam Etching (IBE). (b) AFM images of a grating coupler and (c) a sub-wavelength filter.

Bragg filters, are 100 nm deep etched and fabricated during the same process. The AFM images of a grating coupler and a sub-wavelength Bragg filter Fig. 2 b) and c) reveal sharp edges and low roughness: $<$1 nm on the top and about 2 nm on the sides. Not shown here, the first ring and microdisk resonators fabricated in the YSZ films revealed single-mode behaviors with quality factors up to 10^4. The first YSZ-based filters have an extinction of about 16 dB at 1593 nm with $\Delta\nu_{3dB}$=1.4 nm, completing the passive features available in this innovative platform.

From these optimized processes, we were able to investigate the significance of the metrics: mosaicity, orientation and composition to the propagation losses of YSZ-based waveguides. The central plot Fig. 3 presents the film mosaicity as a function of its thickness for (001) and (111)-oriented types of films. As previously stated, the substrate preparations before growth allows us to promote the (001) or (111) growth direction for thicknesses up to 350 nm, while maintaining a high crystal quality. This result is defined by the light blue window in the central plot of Fig. 3. On the other hand, optical mode simulations yielded a minimum thickness of 250 nm to confine and propagate a single quasi-TE mode in YSZ-based waveguides, with our current process of fabrication. This second result defined another red window in the central plot of Fig. 3. We expected the optimal thickness range for the fabrication of YSZ-based waveguides to be represented by the overlap of both blue and red windows, between 250 and 350 nm. The data shown on the left and right of Fig. 3 are the transmitted light intensity measured from waveguides of different lengths, and whose slope is the propagation losses in dB/cm. As we can see, whatever the growth direction or YSZ doping concentration, the propagation losses measured are about 2 dB/cm in the wavelength range 1300-1600 nm, if the film thickness is between 250 and 350 nm. On the other hand, thicker waveguides revealed higher losses of 11 dB/cm. Thanks to this comparison, we have been able to demonstrate the weak influence of the composition and orientation to the waveguides performances and the clear relationship between film quality (mosaicity) and propagation losses.

B. Yttria-Stabilized Zirconia on silicon

This section reports on the preliminary results regarding the hybrid integration of YSZ on silicon. We applied a design optimization approach to identify the sources of losses in YSZ on silicon waveguides and reduce their contribution. Experimental results of different waveguide geometries are discussed: (i) YSZ directly deposited on silicon waveguides or (ii) YSZ thin film deposited on a flat SOI substrate and then patterned. The former type of design benefits from the well-controlled process of fabrication of the silicon on insulator (SOI) technology, providing high quality and low-losses silicon waveguides, but suffer from a less controlled growth process, as the substrate is not flat and homogeneous. The latter design overcome this obstacle by first depositing YSZ on a perfectly flat and clean SOI substrate and then fabricating the waveguides in the YSZ layer.

To grow epitaxial YSZ on silicon, we employed the so-called two-steps method, extensively studied in the past[24]–[27]. In the first step of this procedure, 10 nm of YSZ is grown at low pressure in the PLD chamber, without oxygen gas at about 10^{-6} Torr. In this reducing environment, YSZ is fed by the oxygen present in the residual native silicon oxides (SiO_x), following the chemical reaction $Zr+2SiO_2 \rightarrow ZrO_2+2SiO$. The remaining SiO phase, being volatile at the growth temperature and low pressure, can be completely removed from the silicon surface. YSZ is then directly facing the silicon lattice and acquires its epitaxial relationship with the substrate. The growth is carried on at higher oxygen pressure of 10^{-4} Torr during the second step of the growth procedure, preventing high oxygen vacancies in the film. The substrate growth temperature is set at 700°C, and the cool down after growth is done under 75 Torr of pure oxygen.

A typical 115 nm thick YSZ film, deposited on a silicon strip waveguide, is presented Fig. II-B with a Transmission Electron Microscopy (TEM) cross-section view. As expected, the electron diffraction patterns revealed a single-oriented YSZ on top of the silicon waveguide, and a polycrystalline phase on the silicon oxides, on both sides of the waveguide. The propagation losses of such a hybrid YSZ on silicon waveguide are above 120 dB/cm at 1350 nm. To explain these large losses, we proposed three mechanisms. First, the polycrystalline phase may contain a large density of defects that can absorb or scatter the light. Second, as the PLD process is extremely directional, gaps open at the interface between the waveguide and the polycrystalline YSZ. The

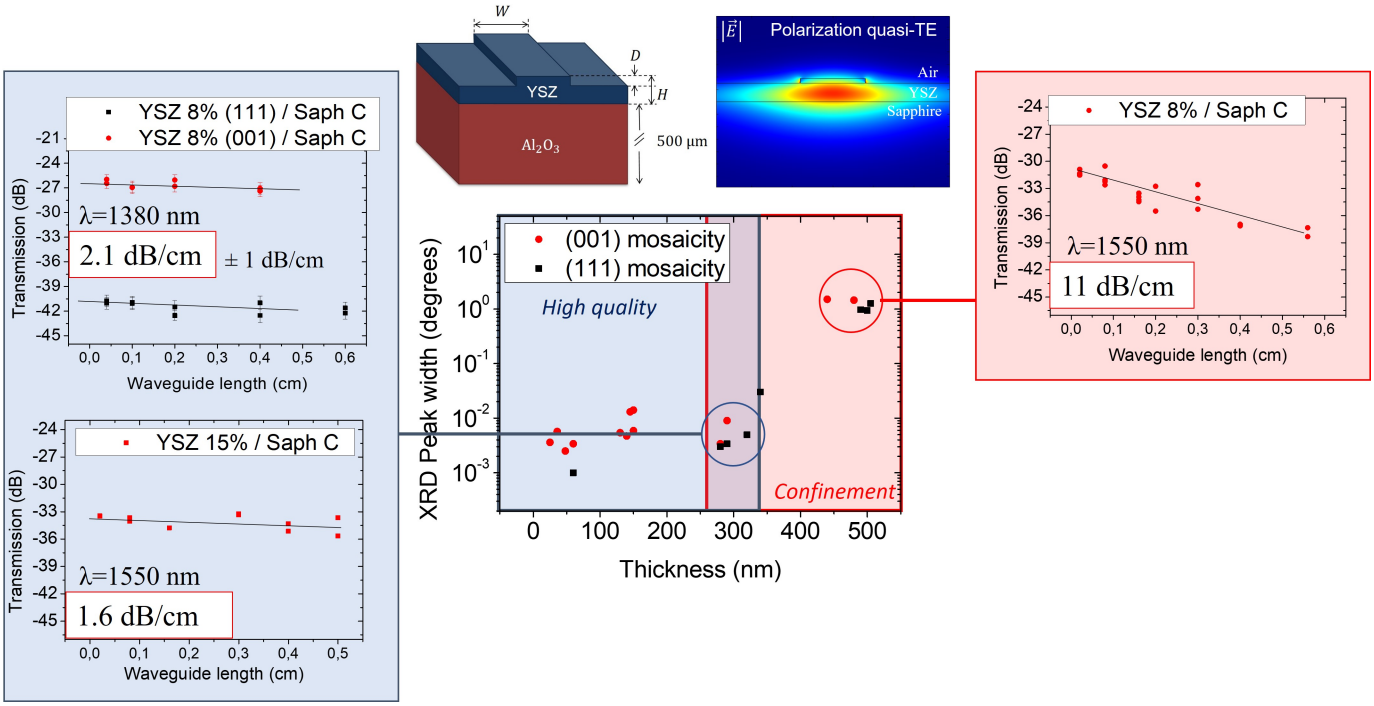

Fig. 3. Propagation losses-thin film quality relationship in YSZ waveguides. (Central plot) The highest quality of YSZ (001) and (111) thin films is obtained for thicknesses ranging from 50 to 350 nm as shown with the blue window. The red window represents the thickness range above 250 nm in which the near-infrared (NIR) light confinement is insured in YSZ waveguides. (Top left) For both (111) and (001) growth direction of YSZ, and (bottom left) for Y_2O_3 doping level of 8%mol and 15%mol, the propagation losses are as low as 1.6 dB/cm for film thicknesses (and waveguide height H) between 250 nm and 350 nm. (Top right) Propagation losses higher than 10 dB/cm are found for the low-quality YSZ films thicker than 350 nm.

dimensions of those gaps might induce light diffraction. Finally, the Energy-Dispersive X-Ray spectroscopy (EDX), performed at the interface between YSZ and silicon, revealed zirconium interdiffusion into the waveguide that could also lead to light absorption or scattering. To test the validity of these mechanisms and quantify their participation to the total losses, we designed, fabricated, and optically measured three hybrid waveguide geometries as shown Fig. 4.

[]

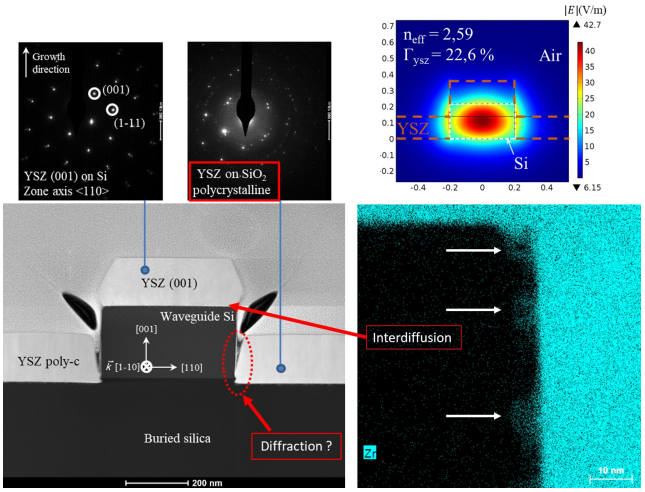

Identification of the three main sources of losses in ¡120 dB/cm YSZ waveguides. While the YSZ crystal is single-oriented when epitaxially grown on the silicon strip waveguides, it is polycrystalline when deposited on amorphous silicon oxide, leading to a higher defects' density. The PLD growth process is very directional and induce shadowing effect. The gap opening on both sides of the Si strip waveguide may induce light diffraction. Energy-dispersive X-ray spectroscopy (EDX) performed in a transmission electron microscope reveals the zirconium interdiffusion in the silicon lattice of the waveguides, increasing the defect density at the YSZ/Si interface.

To keep constant the native silicon oxide thickness before growth, we always prepared the SOI substrate (patterned or not) between 12 and 16 hours before the YSZ deposition. The preparation consists of a wet etching with a 4% hydrofluoric acid solution for a duration ranging from 15 seconds to 4 minutes, depending on the design geometry. At the time of growth, a native silicon oxide thickness of 5 Å is estimated thanks to the oxidation rate of silicon at room temperature and oxygen partial pressure in air[28]. The propagation losses of waveguides at λ=1300 nm have always been measured before substrate preparation (α_i) and after YSZ deposition (α_f), in order to focus on the additional losses $\Delta\alpha = \alpha_f - \alpha_i$ induced by the presence of the YSZ layer in the hybrid YSZ/silicon waveguides. We also characterized the additional losses caused by the substrate preparation: +1 dB/cm for rib waveguides and +3.5 dB/cm for strip waveguides, as well as the PLD process itself without YSZ deposition (only sample loading, heating and YSZ target cleaning): +2.5 dB/cm.

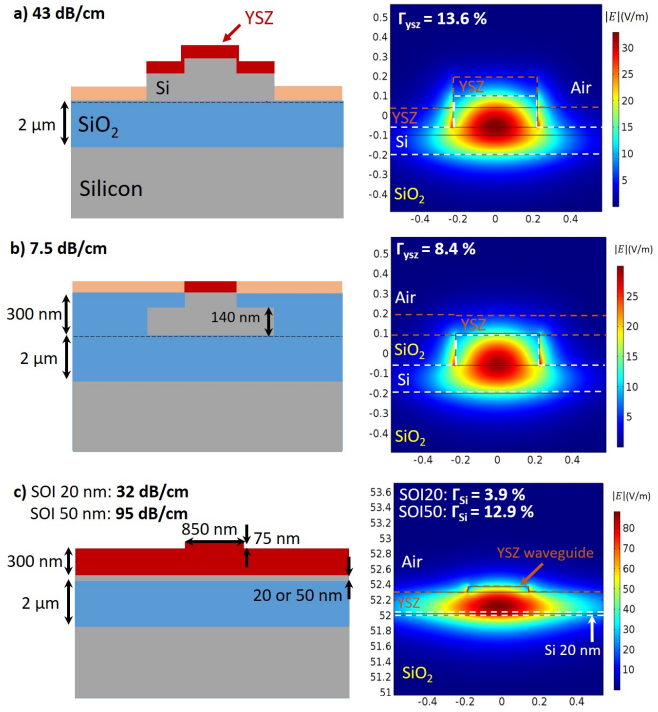

Fig. 4. Three design of hybrid YSZ-on-silicon waveguides with their respective quasi-TE mode simulations and resulting propagation losses. a) The deposition of YSZ on a rib waveguide lower the contribution of the polycrystalline YSZ and diffraction effect to the propagation losses, resulting in 43 dB/cm. b) Buried-silicon waveguide partially exposed during YSZ deposition. The interface YSZ/Si is limited to the top of the waveguide and the propagation losses are the lowest ever reported in hybrid YSZ/Si with 7.5 dB/cm. c) Fabricated YSZ waveguides on thin (20 or 50 nm) silicon-on-insulator (SOI) substrates. The propagation losses is function of the mode overlap with the silicon (Γ_{Si}), 95 dB/cm and $\Gamma_{Si} = 12.9\%$ for 50nm SOI, 32 dB/cm and $\Gamma_{Si} = 3.9\%$ for 20nm SOI. This relationship highlights the strong contribution of interdiffusion-induced interfacial defects in the silicon to the total propagation losses.

The first design, Fig. 4a), aims at characterizing the effect of the polycrystalline YSZ and YSZ gaps, to the waveguide performances. Indeed, as a rib geometry is used instead of a strip geometry, the polycrystalline phase of YSZ is push further from the optical mode. Moreover, the aspect ratio of this design also prevents the formation of gaps on both side of the waveguide. The additional losses for this configuration, with a YSZ layer of 90 nm, are $\Delta\alpha$ = 43 dB/cm, at least 3 times lower than its strip counterpart Fig. II-B. This large improvement is a clear sign than the polycrystalline YSZ and YSZ gaps play a major role in the losses value. However, we can also notice that the rib geometry is naturally less sensitive to the YSZ/Si interfaces than the strip geometry, and that may also contribute to the difference of losses observed. To go further and investigate the participation of these interfaces to the total losses, we turned to the second design, Fig. 4b). A silicon rib waveguide is first buried under a planarized 15 nm silicon oxide layer. SiO_2 is then partially etched down to the top Si waveguide. This configuration limits the YSZ/Si interface to the very minimum, while keeping the local epitaxy of YSZ. The propagation losses are $\Delta\alpha$ = 7.5 dB/cm with 60 nm thick YSZ layer. This is the lowest value ever reported in a YSZ on silicon platform. This confirms the strong influence of the YSZ/Si interface area to the total losses. However, the overlap of the optical mode with the bulk YSZ film has also changed in these designs. This overlap, which represents the ratio of the mode in the YSZ layer as $\Gamma_{YSZ} = \int_{YSZ} Ed^2r / \int_{tot} Ed^2r$, also decreases with the propagation losses, from Γ_{YSZ} = 13.6% for the design Fig. 4 a) to Γ_{YSZ} = 8.4% for the design Fig. 4 b), also suggesting an influence of the bulk of the YSZ film to the losses.

To evidence the role of the bulk YSZ film to the losses and quantify its participation in regard of the YSZ/Si interface, we fabricated a third hybrid waveguides reported in Fig. 4c). In this last design, the optical mode is mostly confined in the YSZ layer. The reduced SOI substrates are prepared by repetitive annealing under oxygen and wet etching before the growth of YSZ and the film is patterned following the process discussed in the previous section. When 300 nm of YSZ is grown on a SOI substrate reduced to 20 nm (substrate named SOI20), the hybrid waveguide losses are 32 dB/cm, lower than the losses of the design Fig. 4a), for which the optical mode was mostly confined in the silicon. To go even further, we increased the silicon thickness to 50 nm (named SOI50) before the YSZ growth. With the same YSZ thickness of 300 nm, the overlap of the mode of the silicon is increased from $\Gamma_{Si} = 3.9\%$ for the SOI20 to $\Gamma_{Si} = 12.9\%$ for the SOI50 while the propagation losses measured are 32 dB/cm for the former and 95 dB/cm for the latter. The linear relationship between Γ_{Si} and the propagation losses evidence the strong effect of the interface to the total propagation losses and that the bulk of the YSZ film is not limiting in this hybrid waveguides. The reduction of the propagation losses below the symbolic value of 1 dB/cm would require the study and the control of the YSZ/Si interface from the epitaxial growth itself or by post-processing step as thermal annealing.

C. Nonlinear Optical properties of YSZ

The low-losses of YSZ waveguides on sapphire allowed us to push further the optical characterization toward the nonlinear optical (NLO) properties[29]. The NLO responses of materials is a promising approach for the development of innovative devices for all-optical data processing, controlled light emission with the generation of supercontinuum or frequency-combs, or to explore quantum phenomena. The capability of YSZ to be grown with different crystalline orientation and stoichiometry motivated our first theoretical approach to characterize the effect of the doping level and distribution to the NLO susceptibility tensor of this material. The resulting theoretical predictions guided us to design the experimental plan. Like silicon, YSZ is a centrosymmetric material exhibiting no second-order optical nonlinearity (i.e. no Pockels effect and second harmonic generation). Then, third order nonlinearity was theoretically and experimentally studied in YSZ waveguides.

We theoretically predicted than the lowest doping concentration would lead the highest third order NLO properties of YSZ [29]. Bearing in mind that a minimum of 8%mol

is required to stabilize the cubic structure, necessary for an efficient use of this oxide as a buffer layer on silicon, we focused our experimental effort on YSZ 8%mol.

To characterize the NLO properties of YSZ 8%mol, we first made a set of waveguides out of a 300 nm thick high-quality YSZ film on sapphire with a Y_2O_3 doping concentration of 8%mol. The waveguides are designed to confine a single quasi-TE mode at the wavelength of 1550nm with an etching depth of 80 nm and width of 760 nm. Experimental propagation losses of 3.2 dB/cm at 1550 nm have been obtained.

The setup used to experimentally characterize the NLO properties of YSZ waveguides is composed of a mode locked erbium-doped fiber laser delivering 150 fs pulses with a repetition rate of f=50 MHz for a wavelength of λ = 1586 nm. More details can been obtained in reference [30]. As expected due to the charge transfer insulator nature of YSZ, with a bandgap of about 4.5 eV, no Two-Photon Absorption (TPA) in YSZ is obtained (Fig. 5 (a)). Indeed, the power collected at the output of the waveguide P_{out} is linearly dependent on the injected input power P_{in}, clearly demonstrating the absence of non-linear absorption. Assuming the transmission coefficients of the sample's facets equal $\kappa_{fa} = \kappa_{fb} = \kappa_f$, one can calculate the transmission coefficient κ_f = 9.1 % from the slope $a = P_{out}/P_{in}$ following

$$a = \frac{1}{\kappa_{fa}\kappa_{fb}e^{-\alpha L}}$$

where α is the propagation losses and L the waveguide length.

The intensity-dependent refractive index (IDRI) Kerr property of YSZ is quantify thanks to the emergence of new frequencies, induced by self-phase modulation mechanism[31], on both sides of the quasi-rectangular shaped laser pump. This phenomenon is observed Fig. 5 b), for incident power higher than 6 mW, and is clearly seen when comparing the low and high-power transmission spectra Fig. 5 c). In absence of TPA, the nonlinear refractive index n_2 can be written as function of the nonlinear phase shift ϕ_{NL} such as

$$\frac{2\pi}{\lambda_0 A_{NL}} n_2 = \phi_{NL}/(\kappa_F P_{in} L_{eff}\eta)$$

with λ_0 the wavelength of the pump, A_{NL} the nonlinear area calculated from the mode simulation and waveguide geometry, $L_{\text{eff}} = (1-\exp(-\alpha L))/\alpha$ the effective length of the waveguide, and $\eta = 1/(F\int_0^{1/F}|U(t)|^2 dt)$ with $U(t)$ the normalized temporal shape of the pulse.

To extract the nonlinearities of YSZ from the experimental data, the contribution of the sapphire substrate is removed taking into account the mode overlap in the two materials. Then, we simulated the experimental spectrum at P_{in} = 11.5 mW Fig. 5 d) to determine the nonlinear phase shift ϕ_{NL}, which yields the nonlinear refractive index n_2 and the corresponding susceptibility defined as $n_2 = 3\chi^{(3)}/4c\varepsilon_0\varepsilon$ with ε the relative dielectric, ε_0 the electric permittivity of vacuum and c the light celerity. More information on the simulation procedure is available here[32], [33]. For the maximum input average power $P_{in} = 11.5$ mW, we obtained a nonlinear phase shift ϕ_{NL} of 15 mrad. This value leads to an effective Kerr nonlinear coefficient in YSZ equals to $n_2^{YSZ} = 4.0 \pm 2 \times 10^{-19}$ m^2W^{-1}, one order of magnitude larger than in sapphire and similar to the one obtained in silicon nitride waveguides [34].

III. Rare-earth doped YSZ

A. The role of rare-earths in light-emitting devices

One other advantage of crystalline oxides and especially YSZ is the possibility to highly dope them with rare-earth to develop on-chip light amplifiers. Indeed, during the last decades, material engineering and integration in silicon-based photonics platform has been developed for this purpose including the use of porous Si[35], Si nanocrystals (Si-nc)[36], Germanium (Ge)-on-Si[37], III-V materials[38] or Erbium (Er^{3+})[39]. The main advantages on rare-earth(RE)-doped oxides integration on Si platforms are the reduced costs in fabrication, not need of specific facilities, high scalability and the possibility of adding other functionalities.

RE emission transitions cover a wide range of wavelengths in the near-IR: Yb_{3+} ($^2F-5/2 \rightarrow {}^2F_{7/2}$) at 1040 nm, Nd_{3+} ($^4F_{3/2} \rightarrow {}^4I_{13/2}$) at 1064 nm, Dy_{3+} ($^6H_{9/2}/{}^6F_{11/2} \rightarrow {}^6H_{5/2}$) at 1300 nm, Pr_{3+} ($^1G_4 \rightarrow {}^3H_5$) at 1300 nm , Tm_{3+} ($^3H_4 \rightarrow {}^3F_4$) 1460 nm and Er^{3+} ($^4I_{13/2} \rightarrow {}^4I_{15/2}$) at 1530 nm [40]. Wavelengths determined by energy transition levels for each RE are characteristic of each element, although variations can occur depending on the structure of the host material [41]. In this direction, we were interested in studying RE emission transitions:$^4I_{13/2} \rightarrow {}^4I_{15/2}$ corresponding to emission wavelength at 1530 for erbium (Er^{3+}) ions. Besides, Er^{3+} characteristic absorption transitions $^4I_{15/2} \rightarrow {}^4I_{9/2}$, $^4I_{15/2} \rightarrow {}^4I_{11/2}$ and$^4I_{15/2} \rightarrow {}^4I_{13/2}$ and its corresponding wavelengths at 800, 980 and 1480 nm are commonly used as pumping wavelengths in Er^{3+} photoluminescence studies[42]. In order to attain optical amplification at a minimum power level, a high concentration of RE is required. Such a concentration normally leads to high ion-ion interaction and ultimately to RE clustering and quenching effects, hindering photoluminescence. Moreover, highly doped oxides with large difference among ionic radii are also prone to reveal high defects density caused by RE ion incorporation to the host decreasing ion emission. In addition, low phononic materials are required to avoid non-radiative pathways for rare-earth ions. Despite these constraints, excellent optical properties have been already demonstrated for a few oxide materials, and light amplification on hybrid photonic integrated circuits have been achieved. Despite in 2019 high material gain (100 dB/cm) was attained from Er^{3+} emission in erbium chloride silicate nanowires [43], hybrid integration of materials such as nanowires on a silicon platform is still challenging. Regarding optical amplification, the same year 2019, the group in Aalto in collaboration with University of Paris-Saclay demonstrated an on-chip Er^{3+} optical amplification at 1533 nm in Al_2O_3 host matrix [44] on Si_3N_4 waveguides with $Er:Al_2O_3$ cladding. In this study, they reported up

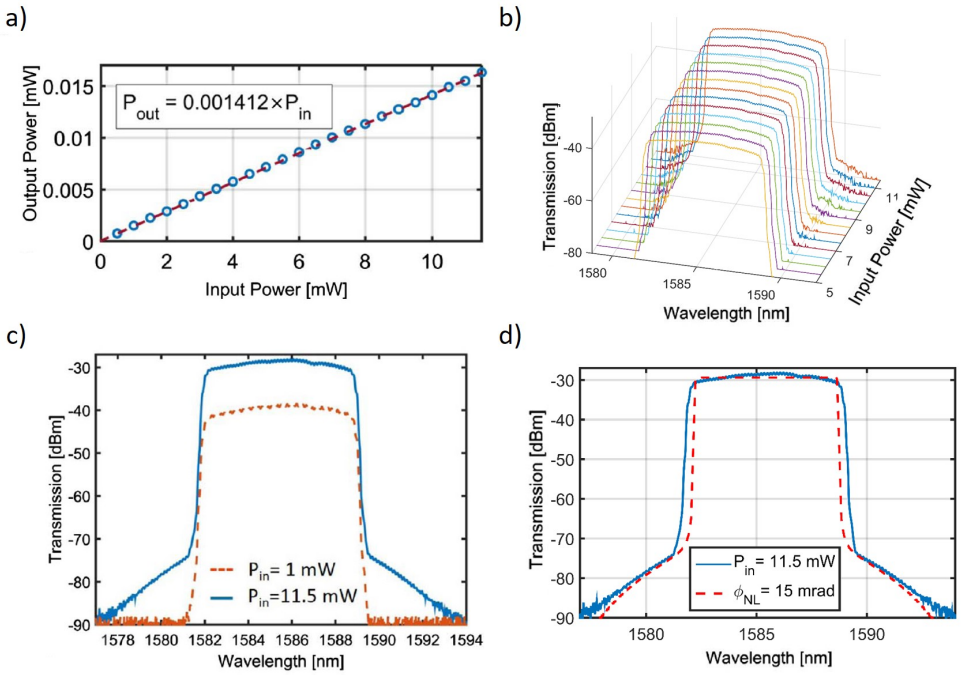

Fig. 5. a) Output power as a linear function of the input power revealing the absence of Two-Photon Absorption (TPA) in a YSZ waveguide. b) Symmetrical broadening of the incident quasi-rectangular shaped pulsed laser induced by self-phase modulation mechanism, derived from the optical Kerr effect. c) Comparison of the transmission spectra at low P_{in} = 1 mW and high P_{in} = 11.5 mW power. d) Simulation of the high-power transmission spectra and determination of the nonlinear phase shift ϕ_{NL}.

to 20.1 ± 7.3 dB/cm net modal gain in 250 μm length waveguides and at least 52.4 ± 13.8 dB/cm of net material gain for 1200 μm waveguides. In 2020, the group of Sonia Garcia-Blanco in University of Twente achieved net gain of 18.1 ± 0.9 dB at 1532 nm for 10 cm Si_3N_4 waveguides with $Er:Al_2O_3$ cladding [45]. The same university had already demonstrated in 2018 erbium-doped potassium double tungstate channel waveguides modal gain of 12 ± 5 dB/cm at 1534 nm wavelength [46]. There are many host approaches for RE-doping materials but the use of crystalline oxides and especially YSZ has been revealed as promising photonic material. Indeed, in addition to the advantages mentioned in the previous sections, its atomic structure includes Y^{3+} with a similar radius than Er^{3+} and its oxygen distribution which is known to play a crucial role in RE emission, makes YSZ a perfect candidate for optical amplification purposes.

B. Monolayer cladding (Er:YSZ)

First, we grow by pulsed laser deposition (PLD) 5 thin film samples of 150 nm thick Er:YSZ monolayer from one sintered PLD target composed by Er^{3+} at different at. % (0.5, 1.5, 3, 5 or 10 at. %) for each target and 8 mol % YSZ. We optically characterized all samples by determining optimal absorption wavelength, establishing optimal Er^{3+} concentration to provide the highest PL intensity and the lowest quenching effects.

As reported in the literature, Er^{3+} ions absorption transitions $^4I_{15/2} \rightarrow ^4I_{9/2}$ and $^4I_{15/2} \rightarrow ^4I_{11/2}$ correspond to 800 and 980 nm emission wavelengths [42]. Despite absorption and emission transitions are the physical characteristics of Er^{3+} ions, its correspondent energy level is host matrix dependent [41]. In this direction, we performed absorption study of our material in the range of 750 and 1000 nm wavelengths using Ti:Sapphire pump laser and measuring by photoluminescence (PL) Er^{3+} emission intensity of $^4I_{13/2} \rightarrow ^4I_{15/2}$ transition at 1530 nm. In Fig. 6(a), we observe optimal absorption at 960 nm corresponding to the Er^{3+} $^4I_{15/2} \rightarrow ^4I_{9/2}$ excitation transition. Then, samples were pumped at a wavelength of 960 nm to attain higher emission at 1530 nm and at 20 mW power for monolayer samples with Er^{3+} concentrations at 0.5, 1.5, 3, 5 and 10 at. % to measure PL emission intensity at 1530 nm. Fig. 6(b) reports the Er^{3+} emission profiles from all monolayer Er:YSZ samples. The highest PL intensity at 1530 nm is found for Er^{3+} at 1.5 at. % followed by 3, 0.5, 5 and 10 at. % Results on PL proved Er^{3+}-Er^{3+} ion interaction for Er^{3+} concentrations higher than 1.5 at.% hinders photoluminescence, while for 0.5 at. % Er^{3+} emission is lower than for 1.5 at.% due to lower number of Er^{3+} nuclei emitters. Optical efficiency study aims to find the sample with lower quenching effects. In this regard, PL intensity normalized for all samples for $^4I_{13/2} \rightarrow ^4I_{15/2}$ transition is measured at a range of pumping powers from 0.5 to 120 mW (Fig.6(c)). Highly optical efficient samples show high ration values in input pumping power and output detected intensity of Er^{3+} emission at 1530 nm. Results in this regard in Fig.6(c) prove high optical efficiency for samples with Er^{3+} concentration doping corresponding to

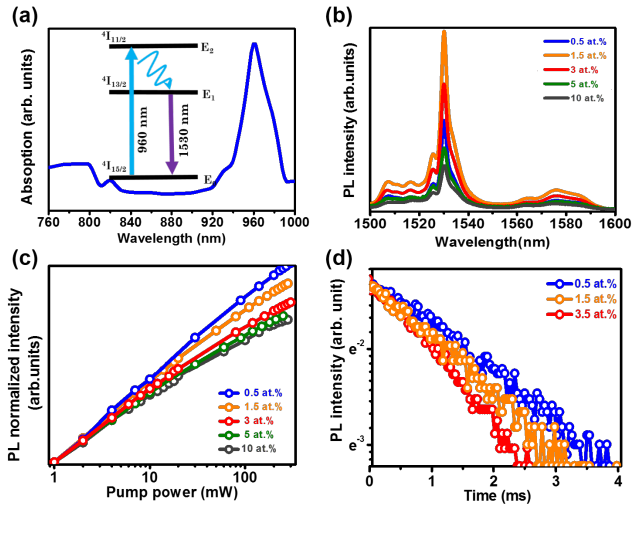

Fig. 6. Optical characterization results by PL of Er:YSZ monolayer samples. (a) Absoption transition study and energy level schematics (inset) of 0.5 at. % Er:YSZ.(b) PL intensity spectra and (c) optical efficiency of 0.5, 1.5, 3, 5 and 10 at. %.(d) Lifetime of 0.5, 1.5 and 3 at. %.

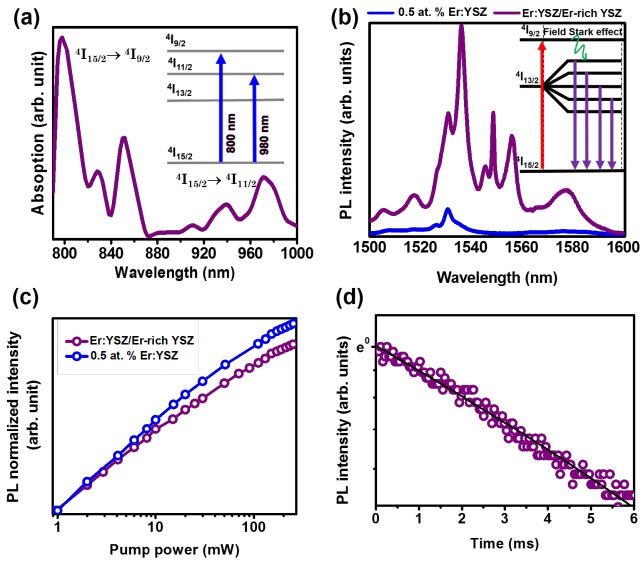

Fig. 7. Optical characterization results by PL of 0.5 at. % Er:YSZ and Er-rich YSZ multilayer sample. (a) Absoption transition study and energy level schematics of the multilayer sample (inset), (b) PL intensity spectra (inset energy level schematics) and (c) optical efficiency of 0.5 at. % Er:YSZ and Er-rich YSZ multilayer sample emission in the near-IR in violet and 0.5 at. % Er:YSZ monolayer in blue.(d) Lifetime of 0.5 at. % Er:YSZ and Er-rich YSZ sample

0.5 at, followed by increasing doping concentration of 1.5, 3, 5 and 10 at % . This behavior reveals 0.5 at. % doping to show low Er^{3+}- Er^{3+}interaction which progressively increases with doping concentration. Long lifetime of Er^{3+} excited state ($^4I_{13/2}$) is also required in order to reach population inversion for optical amplification purposes. We have measured decay time of luminescence of three samples with different Er^{3+} concentration. Besides, we performed direct excitation of the $^4I_{11/2}$ state by PL at room temperature. Fig. 6(d) shows an $^4I_{13/2}$ increase with a decrease of erbium doping concentration. Lifetimes of 2.0, 1.6 and 1.2 ms were obtained for Er:YSZ thin films with Er^{3+} concentrations of 0.5 ,1.5 and 3 at.%, respectively. To conclude, despite 1.5 at. % Er concentration proved the highest PL intensity profile, thin films with 0.5 at.% Er:YSZ revealed lower quenching effects and the largest lifetime.

C. Multilayer cladding (Er-rich YSZ/Er:YSZ)

From optical characterization studies in Er:YSZ monolayers at different Er^{3+} concentrations, a multilayer approach including Er-rich YSZ layers was considered in order to increase PL emission while maintaining high optical efficiency. In this regard, we alternate layers of 0.5 at. % Er:YSZ with of Er-rich YSZ. Er-rich YSZ structure with Er^{3+} $\leq$8 at. % is implemented by PLD with a metallic Er target at $\geq$99.9 % purity. Spectra of PL absorption and emission from multilayer samples show in Fig.7(a) and (b), two different Er^{3+} profiles related to two sites taken by Er^{3+} ions in the YSZ structure [[47]]. A first absorption and emission spectra, optical efficiency and lifetime related to the 0.5 at.% Er:YSZ monolayer structure (Fig. 6) and a second spectra profile characterized by absorption peaks at two wavelengths (Fig. 7(a)) and enhanced PL Er^{3+} emission intensity with presence of Stark splitting effect (Fig. 7(b)), high optical efficiency (Fig. 7(c)) and long lifetime (Fig. 7(d)).

Absorption profile for multilayer sample excited from 750 to 1000 nm wavelengths reveals two absorption transitions: a larger absorption peak at 800 nm and a second at 960 nm wavelength corresponding to the $^4I_{15/2}\rightarrow{}^4I_{9/2}$ and $^4I_{15/2}\rightarrow{}^4I_{11/2}$ transitions, respectively. When exciting multilayer samples composed by Er-rich and 0.5 at. % Er:YSZ layers at 800 nm wavelength and pumping power of 20 mW, an enhanced PL profile showing Stark splitting effect with two maxima at 1530 and 1536 nm are observed (Fig.7 (b)). In Fig.7 (b), PL Er emission spectra from 0.5 at.% Er:YSZ monolayer and 0.5 at. % Er:YSZ/ Er-rich YSZ multilayer samples are compared. Optical efficiency for 1530 nm emission in Er-rich/Er:YSZ YSZ multilayers is slightly lower than for 0.5 at. % Er:YSZ monolayer (Fig.7 (c)). While, the highest lifetime of 3.2 ms was obtained in multilayer samples as shown in Fig.7(d). We demonstrate PL Er^{3+} emission intensity and lifetime is improved by introducing Er-rich layers in 0.5 at. % Er:YSZ sample while optical efficiency at 1530 nm remains moderately lower. Despite quenching effects can be notice by introducing higher concentration of Er^{3+} in the YSZ samples, multilayer structure with Er-rich layers allows Er^{3+} to take other configurations in the YSZ structure revealing different properties than in 0.5 at. % Er:YSZ structure.

D. Er:YSZ hybrid integration on SiN_x waveguides

As silicon waveguides exhibit two photon absorption (TPA) in the near-IR, silicon nitride (SiN_x) was chosen as passive material for guiding light. 600nm thick SiN_x layer was deposited by plasma-enhanced chemical vapor deposition (PECVD) on 1.4 μm thick silicon dioxide (SiO_2). SiN_x waveguides were fabricated in the silicon photonics platform at STMicroelectronics, formed by 248 nm deep-ultraviolet lithography followed by reactive ion etching. Waveguide width was 0.4 μm. SiO_2 was then deposited and chemical mechanical polish (CMP) step was performed to planarize the structure. Planarized waveguides are suitable for the deposition of crystalline cladding of Er-doped YSZ multilayers on an amorphous buried strip waveguide. The resulted structure is an inverse rib waveguide formed by the waveguide and the cladding. Simulations were performed using a two-dimensional (2-D) simulation tool (MODE Solutions from Lumerical, Inc.) to study the optimal thickness of the cladding to maintain the pump mode confined in the SiN_x waveguide while exciting Er^{3+} in the cladding.

SiN_x waveguides allow single-mode propagation of both fundamental modes: quasi-transverse electric (quasi-TE) and quasi-transverse magnetic (quasi-TM) polarization states in the wavelength range from 1.2 to 1.6 μm. From the Er:YSZ cladding simulations, the thickness optimization is carried out simulating single mode propagation at a wavelength of 1530 nm, corresponding to Er^{3+} ions emission. The optimized Er:YSZ thickness is defined as the best trade-off between modal confinement within the SiN_x waveguide core to avoid light leakage in bends and high % of optical power residing in the top Er:YSZ thin film to maximize the excitation of Er^{3+} ions. According to our calculations reported in Fig. (8), the TE guided modes are strongly confined within a waveguide core for a 50 nm thick Er:YSZ layer. In this case ,the power within the active cladding layer is estimated to be 11.46%. In contrast, for a 150 nm thick Er:YSZ layer, guided modes exhibit an improved overlap with the top cladding region which reaches 25.9 %. Finally for 350 nm thickness of Er:YSZ the fraction of optical power in the cladding is of 67.7%, the fundamental quasi-TE mode is highly de-confined from the SiN_x waveguide core. The simulations for TM mode shows 2% of optical power in 50 nm cladding thickness and 8.7% in 150 nm and 29.9 % for thickness of 350nm. Therefore, higher fraction of optical power in active cladding is held for TE than in TM mode.

As expected, the hybrid mode within the SiN_x waveguide and cladding layer raises up to the top cladding as the thickness of Er:YSZ increases. Such a behavior is expected because the refractive index of the Er:YSZ layer ($n_{Er:YSZ}$ = 2.1) is higher than the one of SiN_x (n_SiN_x = 1.9) or in SiO_2 under-cladding (n_{SiO_2} = 1.4) as observed in Fig. 9 for inverse rib system cross-section with and without cladding.

As a conclusion, 150 nm thick Er:YSZ cladding can be considered as an optimal thickness keeping a good trade-off

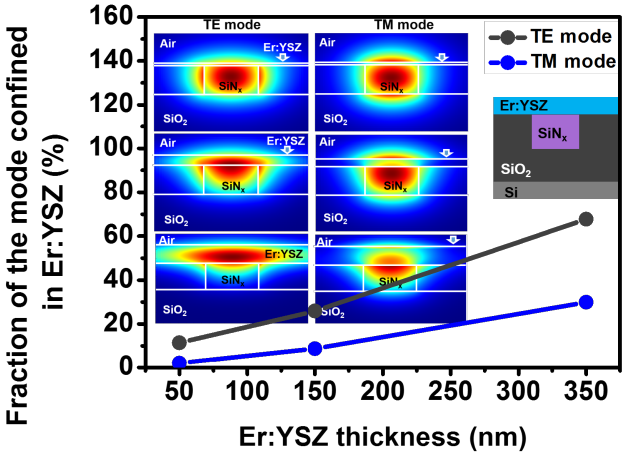

Fig. 8. Graphic of simulated optical power percentage on for TM_{01} and TE_{00} modes related to Er:YSZ/Er-rich YSZ multilayer cladding. Inset schematics, cross-section of SiN_x waveguide buried on SiO_2.Inset simulations, electric field colored map of simulations in TE (left column) and TM (right column) modes on SiN_x waveguide cross-section for cladding thicknesses of 50, 150 and 350 nm.

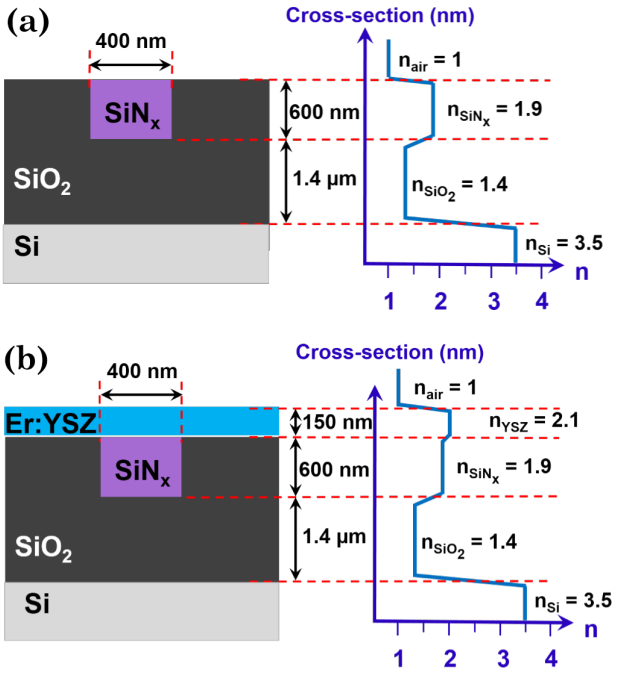

Fig. 9. Geometry of SiN_x waveguide buried on SiO_2 cross-section on the left and graphic of refractive index with dimensions of cross-section for schematics (a) without cladding and (b) Er:YSZ/Er-rich cladding

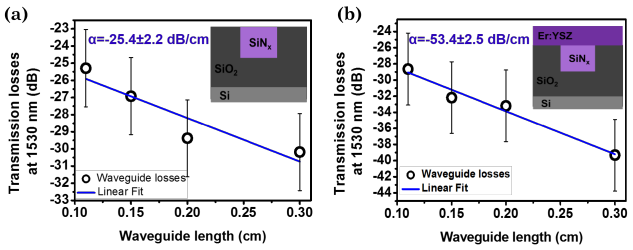

Fig. 10. Absorption and material loss transmission at 1530 nm of four waveguides length and linear fit and insets of schematic SiN_x waveguide buried on SiO_2 for sample (a) without cladding and (b) with 0.5 at. % Er:YSZ/Er-rich YSZ multilayer cladding.

between optical power fraction exciting active cladding and mode confined within the waveguide.

E. Optical gain measurements

Results in optical efficiency, PL emission intensity and simulations on SiN_x waveguides with Er:YSZ proved this material is a good candidate for optical amplification. In this section, we will determine the optical gain of SiN_x waveguides with Er:YSZ multilayer top cladding. First, propagation losses of the SiN_x waveguide and the inverse rib system formed by the SiN_x waveguide and the Er:YSZ cladding were measured (Fig. 10). Propagation losses includes material absorption from SiN_x waveguide which includes H-N bonds and cladding and light scattering from Er:YSZ material interfaces and grain boundaries. Loss measurements were performed by linear fitting the transmission of 4 waveguides of 0.11, 0.15, 0.2 and 0.3 cm at 1530 nm.

Propagation losses as high as -25.4 ± 2.2 dB/cm at a wavelength 1530 nm for SiN_x waveguide system were measured (Fig. 10) due to light leakage to the Si substrate. Adding Er:YSZ top cladding to the waveguides, propagation losses increase up to -53.4 ± 2.5 dB/cm. These characterizations have been performed at a wavelength of 1530 nm and a power of 1 mW. Despite the high propagation losses, we carried out signal enhancement and modal gain experimental measurements. Then, we pumped our waveguides at the absorption wavelength of Er^{3+} (1480 nm). A signal at the Er^{3+} emission wavelength of 1530 nm at a power of 315 μW was also coupled as a probe. Output measurements were analyzed in the optical spectrum analyzer (OSA) for a tuned range of pump power inside the waveguide from 0.5 to 16 mW. Experimental setup in Fig. 11

For all pumping power measurements, signal enhancement at pump wavelength is double checked by calculating the difference between signal pump-on (s_{pumpon}) and pump-off ($s_{pumpoff}$), and by evidencing up-conversion by green light emission in the waveguide length. Furthermore, noise is acquired in probe off state and turned up to be no more than -55 dBm. For increasing pumping power and waveguide equivalent length calculated following the procedure used by

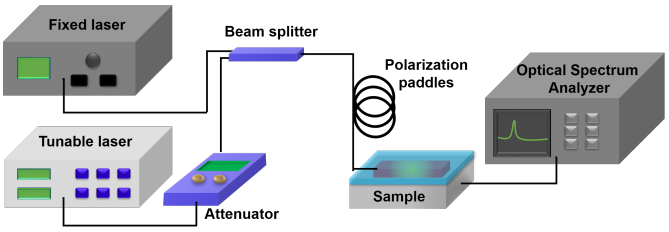

Fig. 11. Optical gain measurement setup: pump fixed laser at 1480 nnm and probe from tunable laser are combine on a beam splitter. After polarization controlled pump and signal are fibered to an optical spectrum analyzer (OSA).

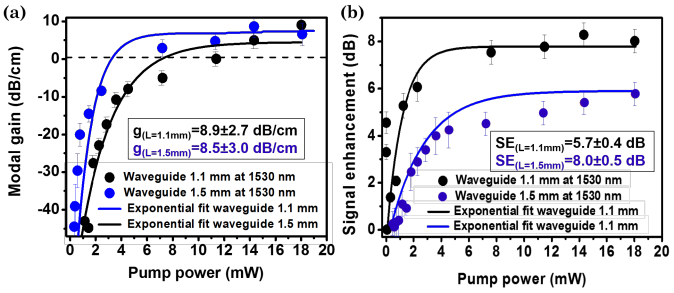

Fig. 12. (a) Modal gain (g_{modal}) and (b) signal enhancement (SE) experimental measurements and exponential fit for multilayer cladding on waveguides lengths of 1.1 and 1.5mm, respectively.

Rönn et al. [44] as,

$$L_{eq} = 2\left(\frac{\eta_{taper}}{\eta_{wg}}\right) + L_{wg}$$

We calculated signal enhancement

$$SE\,(dB) = 10\,log\left(\frac{s_{pumpon}(mw) - ASE(mW)}{s_{pumpoff}}\right)$$

and modal gain

$$g_{mod}\,(dB/cm) = \frac{10}{L_{eq}}\,log\left(\frac{s_{pumpon}(mw) - ASE(mW)}{s_{pumpoff}}\right) - \alpha$$

In which α is referred to the propagation losses. Optical amplification results following equations are analyzed in Fig. 11 for signal enhancement and modal gain. We obtain modal gain of 8.9 ± 2.7 and 8.5 ± 3.0 dB/cm for 0.11 and 0.15 cm long waveguides despite the material absorption and propagation loses. Decreasing modal gain with increasing waveguide length is expected due to material losses. On contrary, signal enhancement is not dependent on material or propagation losses. Thus, signal enhancement increases proportionally to waveguide length as calculated in Fig. 12 (b) with values of 5.7 ± 0.4 and 8 ± 0.5 dB for 0.11 and 0.15 cm waveguides, respectively.

Results on modal gain and signal enhancement for SiN_x waveguides with Er:YSZ top cladding prove this material is a promising host for RE-doping regarding optical amplification purposes in Si-based platform.

IV. Conclusion

More than the results, we aimed in this review to present the method and the tools that we used to successfully develop innovative crystalline oxide-based photonic devices. We demonstrated the potential of material and design optimization approaches for the hybrid integration of crystalline thin films on different platforms, including those of the same nature like oxides on oxide substrates (YSZ on sapphire), oxides on semiconductor (YSZ on silicon) or oxide on amorphous material (YSZ on silicon nitride). For YSZ-based waveguides, we characterized the effect of several thin film's features to the propagation losses and evidenced the preponderant role of the film crystallinity when integrated on sapphire and the substrate-film interface when integrated on silicon. We also experimentally probed the nonlinear optical properties of YSZ waveguides and revealed third-order NLO susceptibilities as high as silicon nitride, in agreement with theory, and inversely proportional to Yttrium doping in YSZ. In addition, we explored YSZ as host material for optical amplification purposes in a silicon-based platform. In this direction, Er^{3+} ions with an emission in the C-band at 1530 nm were implemented in a YSZ matrix grown on a SiN_x waveguide. On a first approach optical characterization aimed to establish optimal Er^{3+} concentration which will provide high PL emission whilst minimizing quenching effects. A second approach searched to engineer Er^{3+} distribution in YSZ thin film by using a multilayer structure including Er-rich layers in the 0.5 at.% Er:YSZ structure. As a result, we increased partially Er^{3+} concentration, thus, PL emission and lifetime increased while avoiding large quenching effects. Modal gain and signal enhancement measured on inverse rib structure formed by multilayer cladding (0.5 at.% Er:YSZ/Er-rich YSZ) and SiN_x waveguides gave values as high as $\sim$9 dB/cm for modal gain and 8 dB for signal enhancement in waveguides of 0.11 and 0.15 cm length, respectively.

V. Acknowledgements

This work has received the funding from the European Research Council (ERC) under the European Union's Horizon 2020 Research and Innovation Program (ERC POPSTAR – grant agreement No 647342) and ANR FOIST project.

VI. Bibliography

References

[1] L. Vivien, L. Pavesi, and S. Pelli, "Silicon photonics and photonic integrated circuits v," in *Proc. of SPIE Vol*, vol. 9891, 2016, pp. 989 101–1.

[2] G. M. Brodnik, S. Liu, M. W. Harrington, D. Bose, M. A. Tran, D. Huang, J. Guo, L. Chang, P. A. Morton, J. E. Bowers, *et al.*, "Ultra-narrow linewidth chip-scale heterogeneously integrated silicon/iii-v tunable laser pumped si/si3n4 sbs laser," in *CLEO: Science and Innovations*, Optical Society of America, 2020, STu3M–5.

[3] B. J. Eggleton, B. Luther-Davies, and K. Richardson, "Chalcogenide photonics," *Nature photonics*, vol. 5, no. 3, pp. 141–148, 2011.

[4] G. Roelkens, A. Abassi, P. Cardile, U. Dave, A. De Groote, Y. De Koninck, S. Dhoore, X. Fu, A. Gassenq, N. Hattasan, *et al.*, "Iii-v-on-silicon photonic devices for optical communication and sensing," in *Photonics*, Multidisciplinary Digital Publishing Institute, vol. 2, 2015, pp. 969–1004.

[5] J. Michel, J. Liu, and L. C. Kimerling, "High-performance ge-on-si photodetectors," *Nature photonics*, vol. 4, no. 8, pp. 527–534, 2010.

[6] P. A. Cox, *Transition metal oxides: an introduction to their electronic structure and properties*. Oxford university press, 2010, vol. 27.

[7] S. Abel, F. Eltes, J. E. Ortmann, A. Messner, P. Castera, T. Wagner, D. Urbonas, A. Rosa, A. M. Gutierrez, D. Tulli, P. Ma, B. Baeuerle, A. Josten, W. Heni, D. Caimi, L. Czornomaz, A. A. Demkov, J. Leuthold, P. Sanchis, and J. Fompeyrine, "Large Pockels effect in micro- and nanostructured barium titanate integrated on silicon," en, *Nature Materials*, vol. 18, no. 1, pp. 42–47, Jan. 2019, Number: 1. (visited on 10/25/2020).

[8] S. Cueff, J. John, Z. Zhang, J. Parra, J. Sun, R. Orobtchouk, S. Ramanathan, and P. Sanchis, "VO $_2$ nanophotonics," en, *APL Photonics*, vol. 5, no. 11, p. 110 901, Nov. 2020. (visited on 08/09/2021).

[9] H. Wang, F. Tang, P. H. Dhuvad, and X. Wu, "Interface enhanced functionalities in oxide superlattices under mechanical and electric boundary conditions," *npj Computational Materials*, vol. 6, no. 1, pp. 1–23, 2020.

[10] M. Bouras, D. Han, S. Cueff, R. Bachelet, and G. Saint-Girons, "Perovskite-Oxide Based Hyperbolic Metamaterials," en, *ACS Photonics*, vol. 6, no. 7, pp. 1755–1762, Jul. 2019, Number: 7. (visited on 10/20/2020).

[11] T. Mizumoto, Y. Shoji, and R. Takei, "Direct Wafer Bonding and Its Application to Waveguide Optical Isolators," en, *Materials*, vol. 5, no. 12, pp. 985–1004, May 2012, Number: 12. (visited on 07/04/2018).

[12] Q. Jia and W. Anderson, "Sputter deposition of yba2cu3o7- x films on si at 500 c with conducting metallic oxide as a buffer layer," *Applied physics letters*, vol. 57, no. 3, pp. 304–306, 1990.

[13] G. Saint Girons, R. Bachelet, R. Moalla, B. Meunier, L. Louahadj, B. Canut, A. Carretero-Genevrier, J. Gazquez, P. Regreny, C. Botella, J. Penuelas, M. G. Silly, F. Sirotti, and G. Grenet, "Epitaxy of SrTiO3 on

Silicon The Knitting Machine Strategy," en, *Chemistry of Materials*, vol. 28, no. 15, pp. 5347–5355, Aug. 2016, Number: 15. (visited on 10/18/2018).

[14] B. Scherrer, S. Heiroth, R. Hafner, J. Martynczuk, A. Bieberle-Hütter, J. L. M. Rupp, and L. J. Gauckler, "Crystallization and Microstructure of Yttria-Stabilized-Zirconia Thin Films Deposited by Spray Pyrolysis," en, *Advanced Functional Materials*, vol. 21, no. 20, pp. 3967–3975, Oct. 2011. (visited on 09/14/2017).

[15] C. López-Gándara, F. M. Ramos, and A. Cirera, "YSZ-Based Oxygen Sensors and the Use of Nanomaterials: A Review from Classical Models to Current Trends," en, *Journal of Sensors*, 2009. (visited on 07/26/2017).

[16] B. A. Boukamp, "Fuel cells: The amazing perovskite anode," en, *Nature Materials*, vol. 2, no. 5, pp. 294–296, May 2003, ISSN: 1476-1122. (visited on 09/06/2017).

[17] D. H. Kim, N. M. Aimon, X. Y. Sun, L. Kornblum, F. J. Walker, C. H. Ahn, and C. A. Ross, "Integration of Self-Assembled Epitaxial BiFeO3–CoFe2O4 Multiferroic Nanocomposites on Silicon Substrates," en, *Advanced Functional Materials*, no. 37, pp. 5889–5896, Oct. 2014. (visited on 09/14/2017).

[18] D. Dubbink, G. Koster, and G. Rijnders, "Growth mechanism of epitaxial YSZ on Si by Pulsed Laser Deposition," en, *Scientific Reports*, vol. 8, no. 1, p. 5774, Dec. 2018. (visited on 08/09/2021).

[19] D. M. Reed, *Microstructure-property relations in solid oxide fuel cells*. University of Missouri-Rolla, 1996.

[20] D. B. Chrisey and G. K. Hubler, *Pulsed Laser Deposition of Thin Films*, en. Wiley, Jun. 1994, Google-Books-ID: 0Oh_QgAACAAJ.

[21] H. M. Christen and G. Eres, "Recent advances in pulsed-laser deposition of complex oxides," en, *Journal of Physics: Condensed Matter*, vol. 20, no. 26, p. 264 005, 2008. (visited on 07/26/2017).

[22] E. V. Loewenstein, "Optical Properties of Sapphire in the Far Infrared*," EN, *JOSA*, vol. 51, no. 1, pp. 108–112, Jan. 1961, Number: 1. (visited on 09/29/2018).

[23] G. Marcaud, S. Matzen, C. Alonso-Ramos, X. Le Roux, M. Berciano, T. Maroutian, G. Agnus, P. Aubert, L. Largeau, V. Pillard, S. Serna, D. Benedikovic, C. Pendenque, E. Cassan, D. Marris-Morini, P. Lecoeur, and L. Vivien, "High-quality crystalline yttria-stabilized-zirconia thin layer for photonic applications," en, *Physical Review Materials*, vol. 2, no. 3, p. 035 202, Mar. 2018. (visited on 07/21/2021).

[24] S. J. Wang, C. K. Ong, L. P. You, and S. Y. Xu, "Epitaxial growth of yittria-stabilized zirconia oxide thin film on natively oxidized silicon wafer without an amorphous layer," en, *Semiconductor Science and Technology*, vol. 15, no. 8, p. 836, 2000. (visited on 10/27/2015).

[25] S. J. Wang and C. K. Ong, "Epitaxial Y stabilized ZrO2 films on silicon: Dynamic growth process and interface structure," *Applied Physics Letters*, vol. 80, no. 14, pp. 2541–2543, Apr. 2002. (visited on 10/27/2015).

[26] P. de Coux, R. Bachelet, C. Gatel, B. Warot-Fonrose, J. Fontcuberta, and F. Sánchez, "Mechanisms of epitaxy and defects at the interface in ultrathin YSZ films on Si(001)," en, *CrystEngComm*, vol. 14, no. 23, p. 7851, 2012, Number: 23. (visited on 11/20/2015).

[27] A. Bardal, T. Matthée, J. Wecker, and K. Samwer, "Initial stages of epitaxial growth of Y stabilized ZrO2 thin films on a SiOx Si(001) substrates," *Journal of Applied Physics*, vol. 75, no. 6, pp. 2902–2910, Mar. 1994, Number: 6. (visited on 11/24/2015).

[28] M. Morita, T. Ohmi, E. Hasegawa, M. Kawakami, and M. Ohwada, "Growth of native oxide on a silicon surface," en, *Journal of Applied Physics*, vol. 68, no. 3, pp. 1272–1281, Aug. 1990, Number: 3. (visited on 03/06/2017).

[29] G. Marcaud, S. Serna, K. Panaghiotis, C. Alonso-Ramos, X. Le Roux, M. Berciano, T. Maroutian, G. Agnus, P. Aubert, A. Jollivet, A. Ruiz-Caridad, L. Largeau, N. Isac, E. Cassan, S. Matzen, N. Dubreuil, M. Rérat, P. Lecoeur, and L. Vivien, "Third-order nonlinear optical susceptibility of crystalline oxide yttria-stabilized zirconia," en, *Photonics Research*, vol. 8, no. 2, p. 110, Feb. 2020. (visited on 07/21/2021).

[30] S. Serna, J. Oden, M. Hanna, C. Caer, X. L. Roux, C. Sauvan, P. Delaye, E. Cassan, and N. Dubreuil, "Enhanced nonlinear interaction in a microcavity under coherent excitation," EN, *Optics Express*, vol. 23, no. 23, pp. 29 964–29 977, Nov. 2015. (visited on 10/08/2018).

[31] "Chapter 10 - Quantum Applications," en, in *Applications of Nonlinear Fiber Optics (Second Edition)*, G. P. Agrawal, Ed., Burlington: Academic Press, Jan. 2008, pp. 447–492. (visited on 08/09/2021).

[32] M. J. Potasek, G. P. Agrawal, and S. C. Pinault, "Analytic and numerical study of pulse broadening in nonlinear dispersive optical fibers," EN, *JOSA B*, vol. 3, no. 2, pp. 205–211, Feb. 1986, Publisher: Optical Society of America. (visited on 08/08/2021).

[33] S. C. Pinault and M. J. Potasek, "Frequency broadening by self-phase modulation in optical fibers," EN, *JOSA B*, vol. 2, no. 8, pp. 1318–1319, Aug. 1985, Publisher: Optical Society of America. (visited on 08/08/2021).

[34] K. Ikeda, R. E. Saperstein, N. Alic, and Y. Fainman, "Thermal and kerr nonlinear properties of plasma-deposited silicon nitride/silicon dioxide waveguides," *Opt. Express*, vol. 16, no. 17, pp. 12 987–12 994, Aug. 2008.

[35] S. Chan and P. M. Fauchet, "Tunable, narrow, and directional luminescence from porous silicon light emitting devices," *Applied physics letters*, vol. 75, no. 2, pp. 274–276, 1999.

[36] L. Pavesi, L. Dal Negro, C. Mazzoleni, G. Franzo, and d. F. Priolo, "Optical gain in silicon nanocrystals," *Nature*, vol. 408, no. 6811, pp. 440–444, 2000.
[37] X. Sun, J. Liu, L. C. Kimerling, and J. Michel, "Room-temperature direct bandgap electroluminesence from ge-on-si light-emitting diodes," *Optics letters*, vol. 34, no. 8, pp. 1198–1200, 2009.
[38] T. Mårtensson, C. P. T. Svensson, B. A. Wacaser, M. W. Larsson, W. Seifert, K. Deppert, A. Gustafsson, L. R. Wallenberg, and L. Samuelson, "Epitaxial iii- v nanowires on silicon," *Nano letters*, vol. 4, no. 10, pp. 1987–1990, 2004.
[39] A. Kenyon, "Erbium in silicon," *Semiconductor Science and Technology*, vol. 20, no. 12, R65, 2005.
[40] ——, "Recent developments in rare-earth doped materials for optoelectronics," *Progress in Quantum Electronics*, vol. 26, no. 4-5, pp. 225–284, 2002.
[41] L. Van Uitert, "Factors influencing the luminescent emission states of the rare earths," *Journal of The Electrochemical Society*, vol. 107, no. 10, p. 803, 1960.
[42] B. Savoini, J. Muñoz-Santiuste, R. Gonzalez, G. Cruz, C. Bonardi, and R. Carvalho, "Upconversion luminescence of er3+-doped ysz single crystals," *Journal of alloys and compounds*, vol. 323, pp. 748–752, 2001.
[43] H. Sun, L. Yin, Z. Liu, Y. Zheng, F. Fan, S. Zhao, X. Feng, Y. Li, and C.-Z. Ning, "Giant optical gain in a single-crystal erbium chloride silicate nanowire," *Nature Photonics*, vol. 11, no. 9, pp. 589–593, 2017.
[44] J. Rönn, W. Zhang, A. Autere, X. Leroux, L. Pakarinen, C. Alonso-Ramos, A. Säynätjoki, H. Lipsanen, L. Vivien, E. Cassan, *et al.*, "Ultra-high on-chip optical gain in erbium-based hybrid slot waveguides," *Nature communications*, vol. 10, no. 1, pp. 1–9, 2019.
[45] J. Mu, M. Dijkstra, J. Korterik, H. Offerhaus, and S. M. Garcıa-Blanco, "High-gain waveguide amplifiers in si 3 n 4 technology via double-layer monolithic integration," *Photonics Research*, vol. 8, no. 10, pp. 1634–1641, 2020.
[46] S. A. Vázquez-Córdova, S. Aravazhi, C. Grivas, Y.-S. Yong, S. M. Garcıa-Blanco, J. L. Herek, and M. Pollnau, "High optical gain in erbium-doped potassium double tungstate channel waveguide amplifiers," *Optics express*, vol. 26, no. 5, pp. 6260–6266, 2018.
[47] H. Omi and T. Tawara, "Energy transfers between er3+ ions located at the two crystalographic sites of er2o3 grown on si (111)," *Japanese Journal of Applied Physics*, vol. 51, no. 2S, 02BG07, 2012.

Alicia Ruiz-Caridad obtained her PhD from University Paris-Saclay, (France) in 2021 on Rare-Earth-doped YSZ materials for optical amplification purposes under the supervision of Prof. Laurent Vivien and Dr. Sylvia Matzen. She joined Centre for Nanoscience and Nanotechnology (C2N) in 2021 as a post-doc to improve and develope Er-doped thin films on optical integrated devices.

Guillaume Marcaud is a postdoctoral researcher, currently in the department of Applied Physics at Yale University working with Dr. Frederick J. Walker and Pr. Charles H. Ahn. He received his M.S. from Sorbonne University and his Ph.D. from Paris-Saclay University under the supervision of Dr. Laurent Vivien and Dr. Sylvia Matzen. He is the author of 12 papers, 1 book chapter and more than 70 presentations in international conferences. His research focuses on the physics of crystalline oxides thin films for photonics, electronics, and quantum applications. He is especially involved in the fabrication of crystalline thin films by pulsed-laser deposition and molecular beam epitaxy, their characterization using synchrotron-based methods, and their integration in nanometer-scale devices.

Elena Durán-Valdeiglesias received the B. Sc degree in Telecomunications Engineering and the Master's degree from Málaga University (Spain) and the Ph. D. degree in physics from the University Paris-Saclay (France). Her work focuses on the integration of carbon nanotubes onto silicon photonic circuits for the realization of active devices.

Joan Manel Ramirez received his PhD from the University of Barcelona, Spain, in 2015, on Si-based light sources. From 2015 to 2018, he joined Paris-South University (France) as a post-doctoral researcher to develop mid-IR photonic integrated circuits. Then, he joined Nokia Bell labs in November 2018 as a member of the technical staff to work on the development of heterogeneous III-V/SOI photonic integrated circuits. Since April 2020, he is the program manager of the heterogeneous III-V/Si integration. His current interests include on-chip transmitters and receivers containing active III-V/Si devices such as lasers, modulators, amplifiers or photodetectors for optical communications. He serves as a reviewer in several peer-reviewed journals including Optica, Optics Express, Applied Physics Letters or the Journal of Selected Topics in Quantum Electronics, among others. He is also member of the topical advisory panel of applied sciences and has authored or co-authored more than 40 journal papers, 50 conference papers, 2 book chapters and 2 patents.

Jianhao Zhang obtained the Ph.D. degree in photonics from Paris-Saclay University and Zhejiang university in 2019. He joined as a post-doc fellow Centre for Nanoscience and Nanotechnology (C2N) in 2020, promoting the research activities in opto-mechanics. His research interests concern cavity opto-mechanics, nonlinear photonics, lasers and interdisciplinary research merging optics and other research fields.

Carlos Alonso-Ramos obtained his PhD in June 2014 at the Universidad de Málaga, Spain, on the development of high-performance integrated photonic circuits for chip interconnects and next generation coherent transceivers. Currently he is a CNRS researcher in the Center for Nanoscience and Nanotechnology (C2N) in Palaiseau,

France. His research interest includes the development of Si photonics devices and circuits in the near- and mid-infrared for applications in telecom, sensing and quantum.

Xavier LeRoux obtained his post as CNRS engineer in the center of Nanoscience and Nanotechnology. His expertise is focused on Silicon photonics structures for photonic applications in clean room. He is author of more than 100 articles.

Ludovic Largeau has been recruited at the CNRS in 1999. He obtained his PhD in 2005 from the University of Poitiers. He is currently a research engineer at C2N, Palaiseau. He manages the platform of structural and chemical analysis of materials. He is an expert of advanced scanning transmission electron microscopy (STEM) and X-Ray diffraction (XRD). His research thematics are focused on the hybridation of heterostructures of III-V, IV-IV semiconductors, crystalline oxides and 2D materials. He is author of 191 articles (h-index : 35) and he has supervised and co-supervised 4 PhD thesis.

Samuel Serna received his degree in physics engineering from the National University of Colombia, Sede Medellin, in 2010 and a double master's degree from the Friedrich-Schiller-University Jena, Germany, in photonics and the Institute d'Optique Graduate School Paris, France, in optics, matter and plasmas" (Erasmus Mundus Master scholarship: Optics in Science Technology -OpSciTech), in 2013. During these studies, he worked in digital in-line holography, diffractive optical elements and integrated photonic devices. He earned his PhD in 2016 at the University of Paris Sud and was postdoctoral researcher at the Centre for Nanoscience and Nanotechnology (C2N-Université Paris-Sud-Université Paris-Saclay) where he designed, fabricated and characterized passive silicon photonics structures and developed novel techniques to test and exploit their third order nonlinear susceptibilities. He was a postdoctoral associate at the Massachusetts Institute of Technology (MIT), where he is explored novel hybrid devices in the integrated photonics platform for telecom and midIR functionalities. Dr. Serna and BSU are part of the LEAP network, bringing industry, government and academia together for the use of integrated photonics and optical technologies. Dr. Serna is an Assistant Professor at Bridgewater Universitz since September 2019.

Nicolas Dubreuil is a Professor at Institut d'Optique Graduate School and at University of Paris-Saclay. His research activities mainly concern the understanding of nonlinear propagation in integrated waveguides and micro-cavities. Following the first demonstration of the enhancement of nonlinear effects due the slow-down of the group velocity in a photonic crystal waveguide, he achieved the first demonstration of the coherent excitation of a nonlinear microcavity. Recently, he has developed a novel technique for the nonlinear characterization of integrated waveguides fabricated with original materials.

Sylvia Matzen received the M.S. degree in materials science in 2008, and the Ph.D. degree in materials science in 2011, both from the Pierre and Marie Curie University (Paris-VI). After a post doc fellowship at the University of Groningen, she joined in 2013 the Paris-Sud University, Orsay, (now Paris-Saclay University since 2019) as assistant professor and the Institute for Fundamental Electronics (now Center for Nanoscience and Nanotechnologies, Palaiseau, since 2016) for research. She is the author of 40 articles, and co-supervised 3 Ph.D. thesis, plus 3 in progress. Her research interests include the epitaxial oxide thin films and their integration in oxide-based electronic devices, with a particular focus on the study of light-matter interactions in ferroelectric materials.

Thomas Maroutian received the M.S. degree in materials science from Lyon University in 1996, and the Ph.D. degree in solid state physics from Paris Diderot University in 2001. Upon joining the French public research center (CNRS) in 2003, he worked at the Institut d'Electronique Fondamentale in Orsay until 2016, and since this date at the Centre for Nanoscience Nanotechnolog in Palaiseau. He is the author of 70 articles, and supervised or co-supervised 7 Ph.D. thesis, plus 3 in progress. His research interests are centered on thin film growth and crystalline oxide integration in electronic and photonic devices.

Eric Cassan has been a Professor at the University of Paris-Sud since 2009. His research topics concern silicon photonics, with a recent shift towards hybrid photonics on silicon for the realization of integrated optical sources and non-linear functions based on third order nonlinear effects.

Philippe Lecoeur received his PhD in solid state physics and materials science from the University of Caen Basse-Normandie in 1994. After two postdoctoral positions at IBM New York and Cogéma-La-Hague, he became assistant professor in 1997 at the University of Caen Basse-Normandie. In 2003, he was recruited as a full professor at the University of Paris-Sud in Orsay, where he joined the Institut d'Electronique Fondamentale, which became the Centre for Nanoscience Nanotechnolog in Palaiseau in 2016, to develop the integration of functional oxides for micro and nanoelectronics. Author and co-author of more than 150 papers, he has supervised 12 PhD students. His main activities are devoted to the development of new electronic functionalities and sensing applications based on thin films of functional oxides.

Delphine Marris-Morini is a Professor at Paris Sud University. Her research interests at the Center for Nanosciences and Nanotechnologies include silicon photonics devices for telecom and sensing applications, both in telecom and mid-IR wavelengths. She received the bronze medal from CNRS in 2013 and an ERC Starting

grant (2015-2020). She published over 100 journal papers.

Laurent Vivien is a CNRS Director of Research at the Centre for Nanoscience and Nanotechnology, a joint Laboratory of CNRS and University of Paris Saclay, France. His research activities focus on the development of fundamental concepts for silicon photonics including optoelectronic and hybrid photonic devices. Since 2016, he has served as Deputy Director of C2N and is in charge of the Photonics Department. He has published over 450 international peer-reviewed journal and conference papers, holds 8 patents and has supervised ¿ 20 PhD and 10 post-docs. In 2015, he obtained an ERC consolidator grant on strained Si Photonics. He is also an elected Fellow of OSA, EOS and SPIE and regularly serves as a Chair of EOS, OSA, IEEE and SPIE conferences on photonics and optoelectronics.